



Micromagnetic Cancer Cell Immobilization and Release for Real-Time Single Cell Analysis



Devina Jaiswal^a, Armin Tahmasbi Rad^a, Mu-Ping Nieh^{a,b,c}, Kevin P. Claffey^d, Kazunori Hoshino^{a,*}

^a Department of Biomedical Engineering, University of Connecticut, Storrs, CT, 06269 USA

^b Department of Chemical and Biomolecular Engineering, University of Connecticut, Storrs, CT 06269, USA

^c Polymer Program, Institute of Materials Science, University of Connecticut, Storrs, CT 06269, USA

^d Department of Cell Biology, University of Connecticut Health Center, Farmington, CT 06030, USA

ARTICLE INFO

Keywords:

Micromagnets
Solenoid
Cell Immobilization
Microfluidic Channel
Cancer cell
Single cell analysis

ABSTRACT

Understanding the interaction of live cells with macromolecules is crucial for designing efficient therapies. Considering the functional heterogeneity found in cancer cells, real-time single cell analysis is necessary to characterize responses. In this study, we have designed and fabricated a microfluidic channel with patterned micromagnets which can temporarily immobilize the cells during analysis and release them after measurements. The microchannel is composed of plain coverslip top and bottom panels to facilitate easy microscopic observation and undisturbed application of analytes to the cells. Cells labeled with functionalized magnetic beads were immobilized in the device with an efficiency of $90.8 \pm 3.6\%$. Since the micromagnets are made of soft magnetic material (Ni), they released cells when external magnetic field was turned off from the channel. This allows the reuse of the channel for a new sample. As a model drug analysis, the immobilized breast cancer cells (MCF7) were exposed to fluorescent lipid nanoparticles and association and dissociation were measured through fluorescence analysis. Two concentrations of nanoparticles, $0.06 \mu\text{g/ml}$ and $0.08 \mu\text{g/ml}$ were tested and time lapse images were recorded and analyzed. The microfluidic device was able to provide a microenvironment for sample analysis, making it an efficient platform for real-time analysis.

1. Introduction

Real time data recording is important for studying live cells. Live cell studies can provide detailed information about cell-cell interaction, receptor-ligand interaction or downstream cellular pathways [1–3]. Studies such as real time apoptosis, cell-substrate interaction have been reported [4,5]. Live cell visualization and data recording often require immunofluorescent markers or nanoparticles such as lipid micelles. These techniques have been employed to study cancer cell signaling pathways, metastasis and cancer targeting in vivo [6,7]. Studies have shown cancer cell functional heterogeneity in a tumor and it is important to study single cells in real time [8,9]. Single cell analysis of cancer cell would give an understanding of cancer initiation, progression and metastasis as well as cellular signaling pathways, which allow us to understand their therapeutic responses [10,11]. Drug screening studies done on single cells can also help target cells more specifically by knocking down some signaling pathways [12].

Single cancer cell studies have been conducted on microfluidic devices or 'Lab on a chip' devices to provide a platform to create the

microenvironment needed to study cellular behavior in a dynamic system [13–16]. These devices were used for various biological assays where sample volumes needed for analysis should be minimized [17]. Important requirements for such devices are that they do not disturb cell-analyte interaction or change cell responses to analytes while immobilizing them in the channel efficiently.

Techniques that have been used to trap single cells in a microfluidic channel include dielectrophoresis (DEP), Polydimethylsiloxane (PDMS) micro traps, microfiltration and immunomagnetic capture [18–21]. Dielectrophoresis can selectively capture cells for applications such as cell fusion studies [22]. PDMS traps in a microfluidic channel can easily immobilize cells for on-chip single cell culture [23]. Physical attributes such as size and stiffness are also used for capturing cancer cells using microfiltration [24]. Even though these techniques have successfully demonstrated the ability to capture cells, there are few drawbacks: PDMS traps disturb uniform flow in the channel and may absorb molecules or nanoparticles under testing [25], and electric fields used in dielectrophoresis may alter cellular activities. Immunomagnetic capture for cell separation [26,27], culture [28],

* Corresponding author.

E-mail address: hoshino@engr.uconn.edu (K. Hoshino).

sorting [29–31] and sifting [32] on a microfluidic platform has been demonstrated. The inclusion of micron sized iron-PDMS posts [33] and pillars [34,35] within microchannel have been studied. Magnets have been integrated within the microfluidic channel as stripes and toothed pattern [36] from paramagnetic [37] and ferromagnetic materials [38], magnetic beads [39] and electroplated metal stripes [40]. In order to magnetize these patterns within the microchannel, an external magnetic field source is applied such as permanent magnet [26] and solenoids [41,42]. These external magnetic field sources either surround the channel or are placed directly on top or bottom of the channel. This makes the device less compatible with commercially available upright or inverted microscopes for long term real time cell analysis. Here we aim to design a simple microfluidic device for effective immunomagnetic cell capture and undisturbed serial sample analysis in a single device in the following way:

1. An array of thin micromagnets was built through minimal fabrication steps to achieve easy cell immobilization. A flat C-shaped solenoid designed to fit most microscopes was used to activate the soft micromagnets and made the process of immunomagnetic immobilization reversible.
2. The use of standard plain coverslips as top and bottom panels, made the microfluidic device simple and useful for general live cell on-chip analysis under either an inverted or upright microscope. The design facilitates addition of reagents under a uniform laminar flow to study captured single cells.

In order to assess real time live cell analysis, we use lipid bilayer nanoparticles as a model drug and quantify cell-nanoparticle interaction [43]. An application of this device is studied using fluorescent nanoparticles (liposomes) that are a potential drug delivery vehicle [44,45]. This analysis provide quantitative information useful in drug testing on rare cancer cells. Nanoparticles being a model for drug delivery, their interaction with cells is of importance in a microfluidic channel as their delivery into the cells can be studied in detail with this device.

2. Materials and methods

2.1. Microchannel fabrication

The schematic in Fig. 1 shows the device design. The main objective is to design a microfluidic device which immobilizes cells without causing additional stress to the cells with high efficiency and enables real time analysis on-chip. The microfluidic device consists of a microfluidic channel, patterned nickel as the micromagnets and an

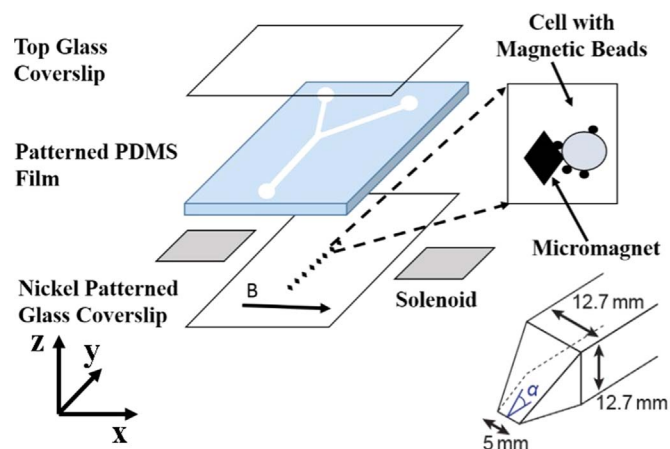


Fig. 1. Schematic of the cancer cell immobilization device with microfluidic channel patterned on a thin PDMS film and enclosed between two coverslips.

external solenoid for active magnetization of micromagnets. The nickel patterns are formed on the bottom substrate to locally enhance the magnetic field generated by the external solenoid. The thin PDMS film with a cut-through pattern of the channel was plasma bonded on the bottom glass substrate such that the nickel pattern was aligned within the channel. Another glass coverslip was plasma bonded on top of the film to seal the channel. Inlet and outlets were made using PDMS blocks. The device was placed between the arms of a C-shaped solenoid. The solenoid produced an external magnetic field that in turn magnetized the nickel pattern. Nickel being a soft magnetic material, was able to magnetize and demagnetize with application or removal of external magnetic field. Nickel micro-pattern, acting as small magnets or micromagnets, enhanced the magnetic field to immobilize cells on the channel. The trapezoid geometry of the solenoid arms was designed to create a focused magnetic field that exerted an addition magnetic force on cells to be pulled towards the nickel pattern.

For nickel magnets, conventional photolithography using a positive photoresist (Microposit S1805) was used to pattern thermally deposited nickel (Kurt J. Lesker, PA, USA) on a glass coverslip as seen in Fig. 2A. Nickel thin film was wet-etched to obtain the micromagnet array (200–250 nm height) of 1000 micromagnets in a single channel. Each micromagnet (Fig. 2, inset) is in a shape of a diamond with an edge size of 64 μm . In order to make a microscope friendly channel that could be used with inverted as well as upright microscopes, thin film channels were designed using PDMS (Dow Corning Sylgard 184, Fisher Scientific) films. The Y shaped channel (0.024 \times 1 mm) was cut on thin PDMS films (thickness:160 and 240 μm) using an electronic design cutting machine (Silhouette Portrait, Silhouette, Utah, USA). The use of the portrait cutter eliminates soft lithography steps that are usually used in conventional microfabrication of PDMS channels. Before the channel was covered with the glass coverslip, the channel was treated with Sigmacote (Sigma Aldrich) to make the surface hydrophobic to prevent cell attachment to glass coverslip. The C-shaped solenoid with 1600 turns, 21 Ω , was developed using low carbon steel bars (0.5 \times 0.5 in. cross section, McMaster Carr, USA). Solenoid arms facing the channel were machined at an edge angle α (see discussion in Section 2.2) to create a 5 mm-wide edge to create focused external magnetic field along the channel. The actual solenoid characterization was done using a Hall Effect sensor (SS490, Honeywell, USA) attached to a mechanical stage located at the center of the solenoid arms.

2.2. Magnetic field analysis

Magnetic separation has been well studied for detection of circulating tumor cells [27,46]. Theory behind magnetization of a soft magnet under an external magnetic field has been described in detail [47]. Briefly, when an external magnetic field H_{ext} is applied, the magnetic dipole of a soft magnetic material align to produce a net magnetization.

Magnetic force (F_m) that acts on a magnetic bead can be calculated as

$$F_m = \frac{N_{\text{bead}} \cdot V \cdot \Delta\chi_{\text{bead}}}{2\mu_0} \nabla B^2 \dots \quad (1)$$

Here, $\mu_0 = 4\pi \times 10^{-7}$, is the magnetic permeability of vacuum, B is the magnetic field intensity, N_{bead} is the number of beads attached to cells, V and $\Delta\chi_{\text{bead}}$ are the volume and effective magnetic susceptibility of the magnetic bead, respectively [48]. We used the value of $\Delta\chi_{\text{bead}} = 0.65$, according to Sinha et al. [48].

COMSOL Multiphysics (version 4.4), AC/DC module was used to simulate the magnetic field produced by the solenoid. The magnetic field generated by solenoid arms with edge angles of $\alpha = 25^\circ$, 45° and 60° was simulated for comparison. Fig. 2B shows the magnetic force acting on a single bead (see Eq. (1)) in z direction plotted for $-6 \text{ mm} < z < 6 \text{ mm}$, considering the edges of the arms to be $z=0$. As shown in

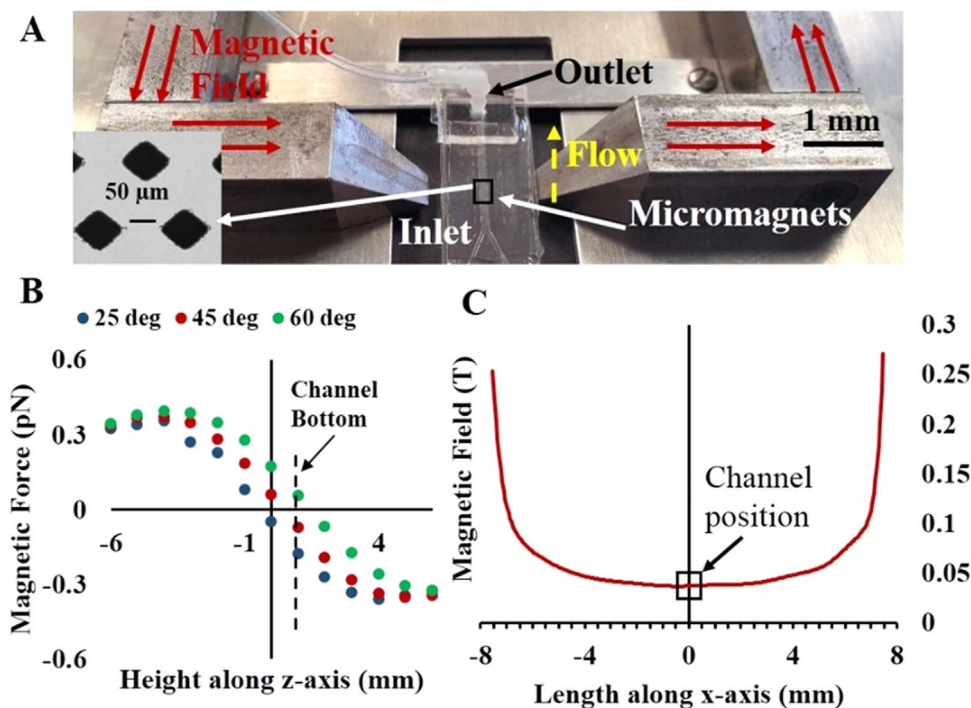


Fig. 2. (A) Microfluidic device was kept between the solenoid arms with flow direction perpendicular to magnetic field direction. Cells attached to functionalized beads were captured at the micromagnets (inset). (B) The magnetic force generated in the z-axis was compared for different α values (25°, 45° and 60°) and the channel was positioned to maximize cell immobilization. (C) The magnetic field intensity between the two poles was plotted and channel was positioned between -0.5 and 0.5 mm along x-axis.

Fig. 2A, the channel is raised by 1 mm to obtain negative forces to move cells in a downward direction. At the channel bottom ($z=1$ mm), cases with $\alpha=25^\circ$ and 45° showed negative force values that can attract cells to the substrate. We used $\alpha=45^\circ$ considering the ease of machining. Fig. 2C shows the magnetic field intensity along x-axis between the two poles. Within the microchannel (-0.5 mm $< x < 0.5$ mm, measured from the center) change in the magnetic field is small.

2.3. Cell culture with magnetic beads

MCF-7 cells (American Type Culture Collection, VA) were cultured in Dulbecco's modified eagle medium (DMEM, Thermo Fisher Scientific), 10% fetal bovine serum (FBS, Thermo Fisher Scientific) and 1% Penicillin/Streptomycin (10,000 U/ml, Thermo Fisher Scientific). Once cells reached 80% confluency, they were trypsinized (Trypsin, Thermo Fisher Scientific) and the cell suspension was used for the experiment. A cell suspension of 250,000 cells/ml was prepared and anti-Epithelial cell adhesion molecule (EpCAM) functionalized polystyrene magnetic beads (JSR Micro, Inc) (3 μ m) were added at a concentration of 5 μ l/ml. The cells are incubated with the magnetic beads for 30 mins at room temperature and 1000 cells are added to the inlet well of the microchannel.

Glass substrates with nickel pattern were seeded with 10,000 cells each and cultured for 3 days in an incubator to test the cytotoxicity of nickel on cells. Cells were trypsinized and trypan blue (Sigma Aldrich) was added to cell suspension to observe difference between live and dead cells.

2.4. Cell Immobilization and release

Cell sedimentation in the channel was measured in the following experiment: Cells were added at a known concentration (C_{cell}) to the channel inlet and microscope was focused at the bottom of the channel. Images were captured every two seconds to account for the number of cells reaching the substrate per second per unit area (S_{cell}). The sedimentation velocity (V_{cell}) of cells was calculated using

$$V_{\text{cell}} = S_{\text{cell}} / C_{\text{cell}} \dots \quad (2)$$

We measured $S_{\text{cell}} = 9$ cells/(s mm²) and C_{cell} was prepared as 833 cells/mm³. From Eq. (2), the calculated V_{cell} was 10.8 μ m/s.

For cell capture, the microchannel was placed between the arms of the solenoid. The whole setup was made on an upright microscope stage for real time cell immobilization imaging. Once the channel was filled with Phosphate-buffered saline (PBS) and air bubbles were removed, cell suspension was added to the inlet. The outlet was connected to the syringe pump that was operated at a withdrawal rate of 15 and 20 μ l/h for 160 and 240 μ m channel, respectively. After cells are added, the external magnetic field created by solenoid (20 V) was switched on to activate the micromagnets. The immobilization experiment was conducted for $n=5$ samples to find the capture efficiency. Each immobilization experiment was conducted for 10 mins and the number of cells entering the channel were counted.

While cells are captured, they will experience the drag force exerted by the fluid flow. The force can be calculated using Stoke's equation:

$$F_{\text{drag}} = 6\pi\mu VR \dots \quad (3)$$

where μ is viscosity of fluid, V is flow velocity, R is radius of cell. The average velocity at 20 μ l/h for 240 μ m is calculated to be $V = 23$ μ m/sec, which gives the drag force on cells to be 5pN.

At the end of this duration, the flow was stopped and the number of cells captured throughout the channel were quantified to calculate the intra-channel immobilization efficiency of the device. Images of the captured cells were obtained to quantify the average number of beads attached to each captured cell. After immobilization, cells are released from the micromagnets by switching off the external magnetic field and introducing higher flow rate of 200 μ l/h.

2.5. Nanoparticles preparation and characterization

1,2-dipalmitoyl-*sn*-glycero-3-phosphocholine (DPPC) and 1,2-dipalmitoyl-*sn*-glycero-3-phospho-(1'-*rac*-glycerol) sodium salt (DPPG) were purchased from Avanti polar lipid without further purification. DPPC and DPPG were dissolved in chloroform in round flask with a

molar ratio of 1:200, and homogenized with NileRed Fluorescent dye (Sigma-Aldrich Chemical co., USA). The NileRed to total lipids molar ratio was 1:200. Then, chloroform was evaporated through a rotary evaporator and was under vacuum at 55 °C for overnight in order to remove residual organic solvent. The sample was hydrated with PBS buffer (pH =7.4) at 25 °C, vortexed and sonicated to reduce the size of the liposomes. Subsequently, liposomes underwent multi-stage (31 passes) extrusion at 58–65 °C through the Mini-Extruder (Avanti polar lipids Inc., USA) using 50 nm polycarbonate filter. The size (hydrodynamic radius, R_{HT}) and size distribution of liposomes was measured using dynamic light scattering (DLS) ALV CGS-3 MD, German) after diluting to the desired concentration (0.1 wt%) in PBS.

2.6. Cell interaction with nanoparticles

Once cells were captured on the micromagnets, nanoparticles (50 nm) were added to the inlet and particles were flown into the channel for 4 mins. The channel was then washed with PBS for next 16 mins. Time lapse images were captured every 30 s for the whole duration of the experiment. To avoid photo bleaching of the sample, a shutter was used to block the excitation light except for duration of 700 ms exposure. The images were analyzed using a custom made program on MATLAB. The fluorescence intensity of the captured cells as well as the fluorescence intensity changes produced by the particle flow in the channel was quantified. Two particle concentrations of 0.06 $\mu\text{g/ml}$ and 0.08 $\mu\text{g/ml}$ at 20 $\mu\text{l/h}$ were tested using the microfluidic channel.

3. Results

3.1. Magnetic field characterization

Solenoid calibration using the Hall Effect sensor at the center position ($x=y=z=0$) between the two arm edges was done to find the relationship between applied voltage and magnetic field generated (Fig. 3A). The magnetic field at the center y - z plane between the arms

was mapped (Fig. 3B). Fig. 3C shows the force (red curve) that acts on a single magnetic bead calculated using Eq. (1) and magnetic field along the z -axis, at $y=0$ position (black arrow in Fig. 3B). Due to external magnetic field, force experienced by the cells is zero at the center position as seen in the graph. The channel is placed 1 mm above the solenoid arm edge so that the cells are pulled down towards the maximum magnetic field region. The z -directional force acting on a single bead was calculated to be 0.11 pN.

The solenoid and micromagnet geometries were modeled with the SolidWorks software (version 2015) and integrated with COMSOL Multiphysics for magnetic field simulation. A magnetization used for the solenoid was such that a uniform magnetic field of 0.038 T was produced at center of the solenoid arms. Nickel was assigned to the micromagnets similar to the actual device. Fig. 4A shows the magnetic field produced by the solenoid and micromagnets. It can be seen that the micromagnets in line with the external magnetic field enhanced the magnetic field by 61.1%. These intensified areas of high magnetic field serve as concentration positions for effective cell capture.

For micromagnet force analysis, ∇B^2 (see Eq. (1)) was calculated using B_x , B_y and B_z along the 0, 10, 25 and 40 μm , in the z direction above the micromagnet. The graph in Fig. 4B shows force versus the distance along the y axis, along the micromagnets (indicated in Fig. 4A, dotted line). The cells will experience maximum magnetic force when they are closest to the micromagnets in the z direction. The magnetic force is 5 times more at 10 μm compared to 40 μm . This shows reduction in force as the cells move away from the base of the microchannel.

3.2. Cell immobilization and release

Cells immobilization efficiency was calculated and compared for all the channels. The immobilization efficiency for 160 and 240 μm channel was 92.2 ± 2.7 and $90.8 \pm 3.6\%$, respectively, for $n=5$ experiments. An average of 439 ± 81 cells entered the channel for the duration for the experiment and 408 ± 83 cells were immobilized by the micromagnets. We used four frames of images to pick up the total

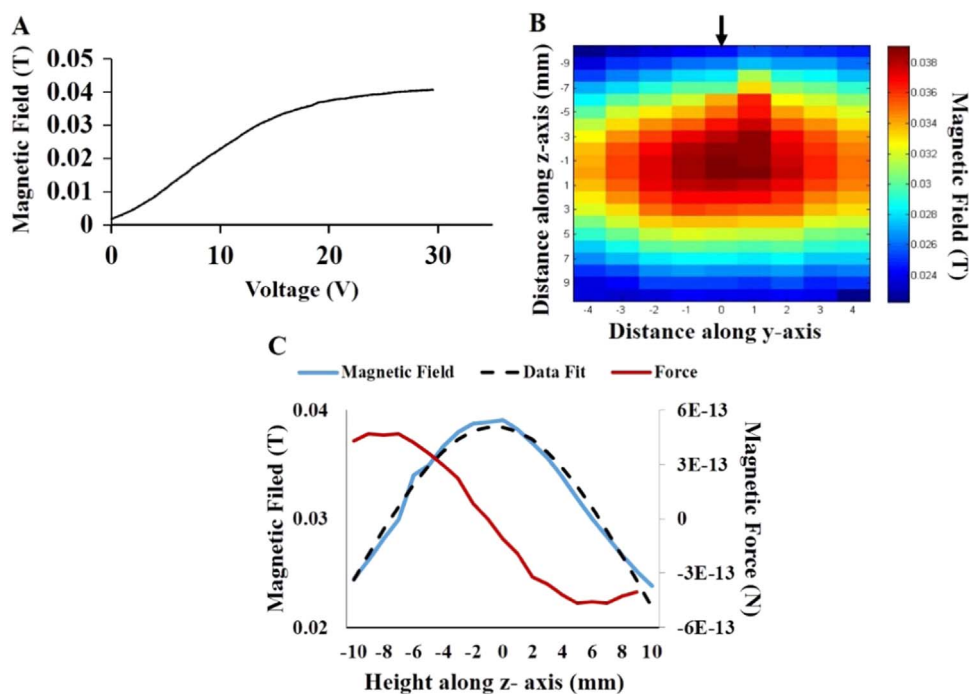


Fig. 3. Characterization of the solenoid magnetic field was done using Hall Effect sensor. (A) The magnetic field at the center position of the two arms was calibrated with increase in voltage. (B) A $20 \times 8 \text{ mm}^2$ area was scanned at operating voltage of 20 V in the yz -direction to map the magnetic field distribution between solenoid arms. The center was found to have maximum magnetic field than the edges. (C) Magnetic force (red) calculated at center of the solenoid arms along z -axis. (For interpretation of the references to color in this figure legend, the reader is referred to the web version of this article.)

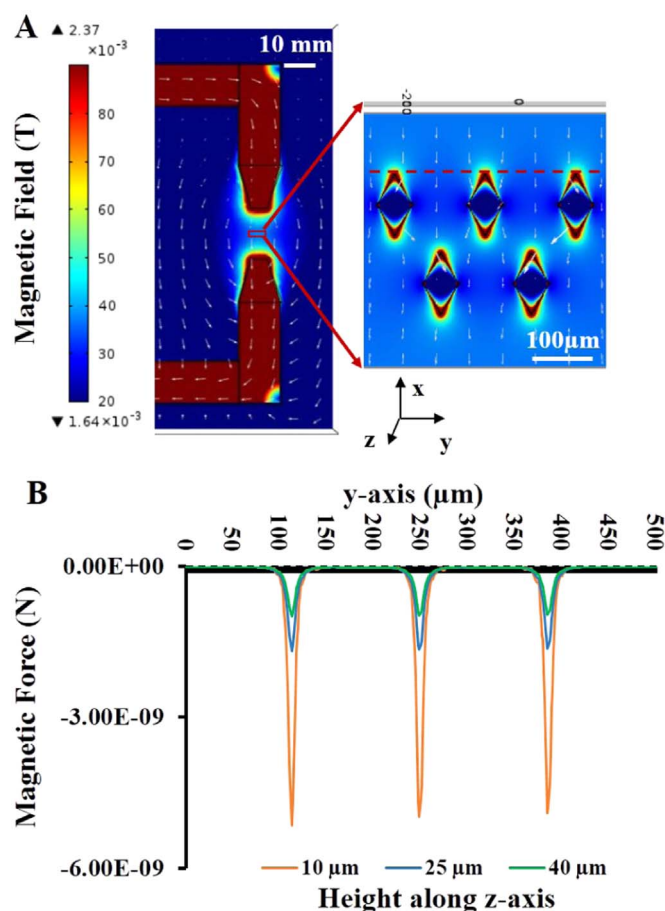


Fig. 4. (A) COMSOL simulation showed micromagnet edge aligned with the external magnetic field acted as the enhanced magnetic field area for cell capture. (B) Force analysis showed that the cells experienced maximum magnetic field when they were close to the micromagnets. With increase in height away from the micromagnets, the downward pulling force also reduces.

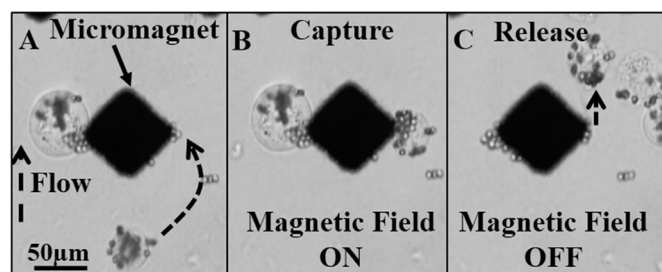


Fig. 5. As the cells suspension passed through the channel with the flow (A), the cells experienced a higher localized magnetic field at the micromagnets. This field attracted them to get temporarily immobilized on channel surface (B). Once the magnetic field was turned off, the cells were released from its immobilized state and channel was cleared for next sample (C). Both the cells seen immobilized in B are release in C.

of 100 captured cells to count the number of beads per cell. The average number of magnetic beads per cell was found to be 5 ± 2 . Out of the 100 cells counted, 35% cells consisted of three or less magnetic beads. Cell release was quantified depending on the number of cells that were released once external magnetic field was switched off and the flow rate was increased. Cells release was achieved after the external magnetic field was turned off and higher flow rate was introduced to clear the channel faster for serial sample analysis. The images in Fig. 5 show the sequences of cell capture and release. Fig. 5A shows cell moving towards the micromagnet, being captured at the micromagnet (Fig. 5B) and finally being released (Fig. 5C) from the immobilized state when magnetic field is removed.

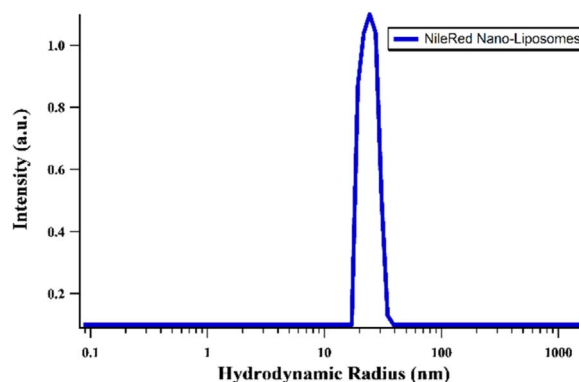


Fig. 6. Dynamic light scattering result which shows the size distribution of nanoliposomes. The hydrodynamic radius, R_H of lipid spherical carriers after encapsulation of fluorescent dyes was 23.1 nm and the result demonstrates monodispersity of the nanoparticles.

3.3. Nanoparticle Characterization

DLS results (Fig. 6) showed a monodispersed liposomes with a peak R_H of ~ 23.1 nm corresponding to the half of the filter size. Most importantly, DLS data clearly indicated the absence of nanoparticle aggregation in the solution. Moreover, there is no sub-5-nm particle seen in the solution, implying the absence of free NileRed molecules. Therefore the obtained fluorescent signals were primarily attributed to the encapsulated liposomes.

3.4. Nanoparticle Cell interaction Study

Cancer cell interaction with liposomes can be seen in Fig. 7A-E. Fig. 7A, B, C, D shows time points 2, 4, 6 and 16 mins, respectively. Cells captured on micromagnets show no fluorescence for the first 2 mins. When particles were added after 2 mins, fluorescence can be seen in the channel as well as within cells from 2.5 to 6.5 mins. Wash starts at 6.5 mins and clears the channel to reduce particle related fluorescence in the channel whereas cells still show accumulation of particles. The channel fluorescence intensity closest to the cells was used as particle concentration in the channel for analysis. Cell and channel intensity was measured using MATLAB by forming a virtual box around the target cells and background area within few microns from the target cell as seen in Fig. 7E, white boxes show the cell intensity and yellow boxes represent the area selected for background analysis. Fig. 7F shows the fluorescence intensity plots versus time for nanoparticles of two concentrations, 0.6% and 0.8%, with 20 $\mu\text{l/h}$ flow rate.

Channel fluorescence values (Fig. 7F, blue plots) were converted to concentration values using concentration and fluorescence intensity standard curve. An increase after 2.5 mins (Fig. 7F, indicated by T_1) and a decrease after 8 min is observed in particle concentration in the channel. The time delay is attributed to the time for particles to travel to the observation site. The delay time for the clearance of nanoparticle through the wash buffer, which was introduced into the channel at 6.5 min (Fig. 7F, T_2) was also observed for the same reason. Cell fluorescence intensity (red plots) also undergoes a rise after 2.5 min time point but retains fluorescence with a slight decrease.

4. Discussion

The microfluidic device designed and fabricated in this study provides high live cell immobilization efficiency. A wide range of efficiencies in antibody mediated cell capture has been reported, ranging from more than 30–95% [13]. The micromagnets along with the focused external magnetic field in this study were able to immobilize cells with high efficiencies of 90–92%. The technique of

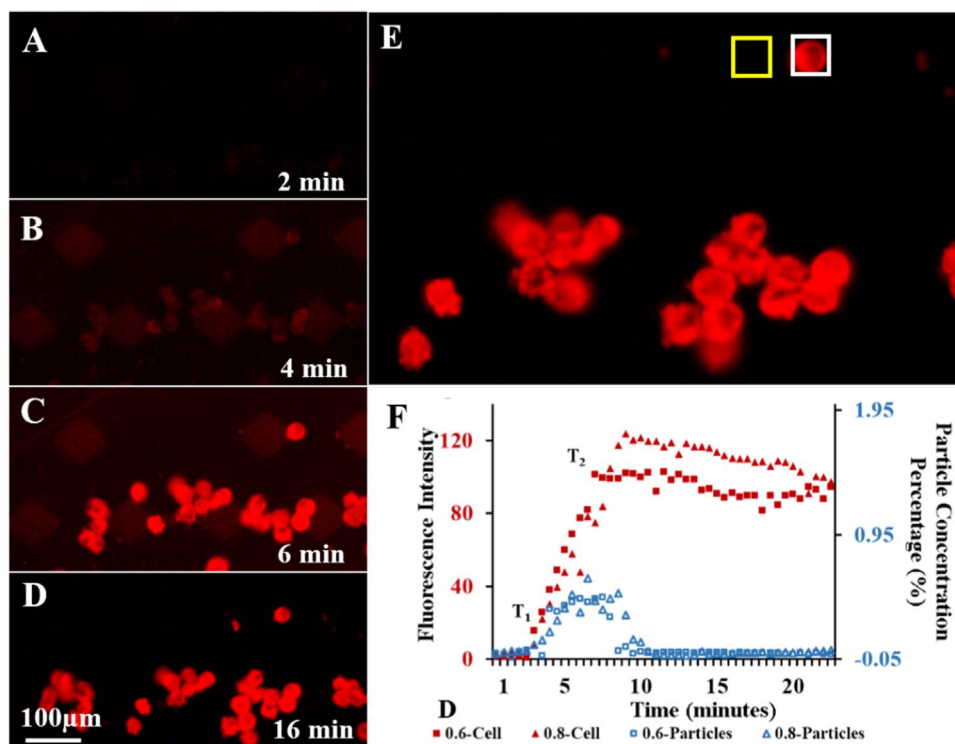


Fig. 7. Nanoparticle interaction with cells immobilized in the channel was recorded using time lapse images. (A) Initially there was no fluorescence recorded in the channel. (B) After pulse nanoparticle input was given, the cells gradually started fluorescing showing nanoparticle-cell interaction. The fluorescence increased with time (C) and after the channel was washed the cells retained their fluorescence (D). (E) For analysis, fluorescence intensity of the single cells and channel fluorescence intensity close to that cell was quantified. (F) The experimental data shows an increase in fluorescence intensity after particles are introduced into the channel ($T_1=2.5$ min). When channel is washed ($T_2=6.5$ min), the channel intensity (blue plots) drops gradually with flow but the cells (red plots) retain the fluorescence with a slight decrease over time. (For interpretation of the references to color in this figure legend, the reader is referred to the web version of this article.)

immunomagnetic capture on nanometer thickness nickel pattern allows cells to be trapped without physical hindrance in a flow chamber or a large electric field as in previously reported methods [25]. Nickel is a soft magnet, non-toxic material and it has been used for various biomedical applications [49]. Nickel film showed no visual toxicity when cells were cultured on the patterned glass substrate for 3 days and a viability percentage of $86.42 \pm 4.65\%$ was obtained. Studies have shown low remnant magnetism for nickel nanoplates and nanowires [50,51]. Even though nickel shows slight remanence magnetism, the device can be easily flushed when external magnetic field is removed and a faster flow is applied.

Along with immobilization of cells, analysis including cell stimulation or cell-cell interaction [52] is equally important. The real-time single cell analysis allows us to monitor the trapped cells in an optically clear field for visualization and data recording. Even though PDMS is a widely used material for microfluidic devices, this material has high diffusivity to materials such as nanoparticles and fluorescent dyes [53]. The glass coverslip top and bottom panel avoids presence of PDMS either in the flow path or in the light path. Thin PDMS film was only used for channel walls which did not affect nanoparticle cell interaction data. Due to thin film handling convenience, 240 μm-height channel was used for nanoparticle cell interaction study.

Nanomaterials such as liposomes have been used in biomedical engineering for phototherapy, imaging and drug delivery [54]. Drugs can be entrapped inside or within the phospholipid bilayer of the liposomes [55]. In this study, fluorescent nanoparticles were used to study the interaction with immobilized cells in a microfluidic channel. The reaction model is analogous to surface plasmon resonance (SPR) biosensor analysis [56], where molecular interaction is studied by immobilizing a reactant in the device and its interaction with suspended reactant is monitored. Here, we immobilized cells and nanoparticles flow in a channel allowing cell-particle interaction, which

can be recorded in real time for analysis.

5. Conclusion

In conclusion, the designed microfabricated device can be reused for serial sample analysis and provides an optically clear path for real time fluorescence microscopy without absorption of fluorescent agents in PDMS. The device is able to provide statistically relevant data which is difficult for devices on which only one cell can be studied at a time. Interaction of immobilized cells with liposomes was analyzed in real time for two concentrations. Device geometry enabled pulsed dose of analyte to the cells in a time-controlled manner.

Acknowledgements

The authors acknowledge the National Science Foundation (NSF IDBR: 1555986) for financial support. We also thank Dr. Leslie Shor of University of Connecticut and her group members for giving access to microfabrication equipment and fruitful advice. Mu-Ping Nieh and Armin Tahmasbi Rad would like to thank the support from NSF-CBET 1605971.

References

- [1] C. Gales, R.V. Rebois, M. Hogue, et al., Real-time monitoring of receptor and G-protein interactions in living cells, *Nat. Methods*. 2 (3) (2005) 177–184.
- [2] P. Zhu, S.H. Baek, E.M. Bourk, et al., Macrophage/cancer cell interactions mediate hormone resistance by a nuclear receptor derepression pathway, *Cell* 124 (3) (2006) 615–629.
- [3] M. Rehm, H. Dubmann, J.H.M. Prehn, Real-time single cell analysis of Smac/DIABLO release during apoptosis, *J. Cell Biol.* 162 (6) (2003) 1031–1043.
- [4] G. Seisenberger, M.U. Ried, T. Endress, H. Buning, M. Hallek, C. Brauchle, Real-time single-molecule imaging of the infection pathway of an adeno-associated virus, *Science* 294 (5548) (2001) 1929–1932.
- [5] V. Yashunsky, V. Lirtsman, M. Golosovsky, D. Davidov, B. Aroeti, Real-time

- monitoring of epithelial cell-cell and cell-substrate interactions by infrared surface plasmon spectroscopy, *Biophys. J.* 99 (12) (2010) 4028–4036.
- [6] X. Michalet, F.F. Pinaud, L.A. Bentolila, et al., Quantum dots for live cells, in vivo imaging, and diagnostics, *Science* 307 (5709) (2005) 538–544.
- [7] M.W. Ward, M. Rehm, H. Duessmann, S. Kacmar, C.G. Concannon, J.H.M. Prehn, Real time single cell analysis of bid cleavage and bid translocation during caspase-dependent and neuronal caspase-independent apoptosis, *J. Biol. Chem.* 281 (9) (2006) 5837–5844.
- [8] D.L. Dexter, E.N. Spemulli, Z. Fligiel, et al., Heterogeneity of cancer cells from a single human colon carcinoma, *Am. J. Med* 71 (6) (1981) 949–956.
- [9] L. Weiss, Cancer cell heterogeneity, *Cancer Metastas. Rev.* 19 (3) (2000) 345–350.
- [10] D. Wang, S. Bodovitz, Single cell analysis: the new frontier in omics, *Trends Biotechnol.* 28 (6) (2010) 281–290.
- [11] J.M. Irish, R. Hovland, P.O. Krutzik, et al., Single cell profiling of potentiated phospho-protein networks in cancer cells, *Cell* 118 (2) (2004) 217–228.
- [12] P.O. Krutzik, J.M. Crane, M.R. Clutter, G.P. Nolan, High-content single-cell drug screening with phosphospecific flow cytometry, *Nat. Chem. Biol.* 4 (2) (2008) 132–142.
- [13] R.N. Zare, S. Kim, Microfluidic platforms for single-cell analysis, *Annu Rev. Biomed. Eng.* 12 (1) (2010) 187–201.
- [14] J. Chen, J. Li, Y. Sun, Microfluidic approaches for cancer cell detection, characterization, and separation, *Lab Chip*. 12 (10) (2012) 1753–1767.
- [15] J. Chung, H. Shao, T. Reiner, D. Issadore, R. Weissleder, H. Lee, Microfluidic cell sorter (μ FCS) for on-chip capture and analysis of single cells, *Adv. Healthc. Mater.* 1 (4) (2012) 432–436.
- [16] van den Brink, T.G. Floris, E. Gool, J. Frimat, J. Bomer, A. van den Berg, S. Le Gac, Parallel single-cell analysis microfluidic platform, *Electrophoresis* 32 (22) (2011) 3094–3100.
- [17] V. Lecault, A.K. White, A. Singhal, C.L. Hansen, Microfluidic single cell analysis: from promise to practice, *Curr. Opin. Chem. Biol.* 16 (3–4) (2012) 381–390.
- [18] J. Voldman, Electrical forces for microscale cell manipulation, *Annu Rev. Biomed. Eng.* 8 (1) (2006) 425–454.
- [19] S.L. Faley, M. Copland, D. Wlodkowic, et al., Microfluidic single cell arrays to interrogate signalling dynamics of individual, patient-derived hematopoietic stem cells, *Lab a Chip* 9 (18) (2009) 2659–2664.
- [20] S. Zheng, H. Lin, J. Liu, et al., Membrane microfilter device for selective capture, electrolysis and genomic analysis of human circulating tumor cells, *J. Chromatogr. A* 1162 (2) (2007) 154–161.
- [21] T. Deng, M. Prentiss, G.M. Whitesides, Fabrication of magnetic microfiltration systems using soft lithography, *Appl Phys. Lett.* 80 (3) (2002) 461–463.
- [22] A.M. Skelley, O. Kirak, H. Suh, R. Jaenisch, J. Voldman, Microfluidic control of cell pairing and fusion, *Nat. Meth.* 6 (2) (2009) 147–152.
- [23] D.D. Carlo, L.Y. Wu, L.P. Lee, Dynamic single cell culture array, *Lab a Chip* 6 (11) (2006) 1445–1449.
- [24] Y. Tang, J. Shi, S. Li, L. Wang, Y.E. Cayre, Y. Chen, Microfluidic device with integrated microfilter of conical-shaped holes for high efficiency and high purity capture of circulating tumor cells, *Sci. Rep.* 4 (2014) 6052.
- [25] M. Kirschbaum, M.S. Jaeger, C. Duschl, Correlating short-term Ca²⁺ responses with long-term protein expression after activation of single T cells, *Lab a Chip* 9 (24) (2009) 3517–3525.
- [26] S.B.N. Gourikutty, C. Chang, P.D. Puii, Microfluidic immunomagnetic cell separation from whole blood, *J. Chromatogr. B* 1011 (2016) 77–88.
- [27] K. Hoshino, Y. Huang, N. Lane, et al., Microchip-based immunomagnetic detection of circulating tumor cells, *Lab a Chip* 11 (20) (2011) 3449–3457.
- [28] J.H. Kang, S. Krause, H. Tobin, A. Mammoto, M. Kanapathipillai, D.E. Ingber, A combined micromagnetic-microfluidic device for rapid capture and culture of rare circulating tumor cells, *Lab a Chip* 12 (12) (2012) 2175–2181.
- [29] D. Horak, Z. Svobodova, J. Autebert, et al., Albumin-coated monodisperse magnetic poly (glycidyl methacrylate) microspheres with immobilized antibodies: application to the capture of epithelial cancer cells, *J. Biomed. Mater. Res. Part A* 101 (1) (2013) 23–32.
- [30] J. Autebert, B. Coudert, J. Champ, et al., High purity microfluidic sorting and analysis of circulating tumor cells: towards routine mutation detection, *Lab a Chip* 15 (9) (2015) 2090–2101.
- [31] A.E. Saliba, L. Saias, E. Psychari, et al., Microfluidic sorting and multimodal typing of cancer cells in self-assembled magnetic arrays, *Proc. Natl. Acad. Sci. USA* 107 (33) (2010) 14524–14529.
- [32] C.M. Earhart, C.E. Hughes, R.S. Gaster, et al., Isolation and mutational analysis of circulating tumor cells from lung cancer patients with magnetic sifters and biochips, *Lab a Chip* 14 (1) (2014) 78–88.
- [33] M. Faivre, R. Gelszinnis, J. Degouttes, et al., Magnetophoretic manipulation in microsystem using carbonyl iron-polydimethylsiloxane microstructures, *Biomicrofluidics* 8 (5) (2014) 054103.
- [34] X. Yu, R. He, S. Li, et al., Magneto-Controllable capture and release of cancer cells by using a micropillar device decorated with graphite oxide-coated magnetic nanoparticles, *Small* 9 (22) (2013) 3895–3901.
- [35] Y. Liu, S. Guo, Z. Zhang, et al., A micropillar-integrated smart microfluidic device for specific capture and sorting of cells, *Electrophoresis* 28 (24) (2007) 4713–4722.
- [36] W. Liu, N. Dechev, I.G. Foulds, R. Burke, A. Parameswaran, E.J. Park, A novel permalloy based magnetic single cell micro array, *Lab a Chip* 9 (16) (2009) 2381–2390.
- [37] C. Sun, H. Hassanisaber, R. Yu, S. Ma, S.S. Verbridge, C. Lu, Paramagnetic structures within a microfluidic channel for enhanced immunomagnetic isolation and surface patterning of cells, *Sci. Rep.* 6 (2016) 29407.
- [38] S. Kim, S. Han, M. Park, et al., Circulating tumor cell microseparator based on lateral magnetophoresis and immunomagnetic nanobeads, *Anal. Chem.* 85 (5) (2013) 2779–2786.
- [39] V. Sivagnanam, B. Song, C. Vandevyver, J.G. Bunzli, M.A.M. Gijs, Selective breast cancer cell capture, culture, and immunocytochemical analysis using self-assembled magnetic bead patterns in a microfluidic chip, *Langmuir* 26 (9) (2010) 6091–6096.
- [40] D.W. Inglis, R. Riehn, R. Austin, J. Sturm, Continuous microfluidic immunomagnetic cell separation, *Appl Phys. Lett.* 85 (21) (2004) 5093–5095.
- [41] C.W. Yung, J. Fiering, A.J. Mueller, D.E. Ingber, Micromagnetic-microfluidic blood cleansing device, *Lab a Chip* 9 (9) (2009) 1171–1177.
- [42] M. Donolato, A. Torti, N. Kostesha, et al., Magnetic domain wall conduits for single cell applications, *Lab a chip* 11 (17) (2011) 2976–2983.
- [43] C. Gräfe, A. Weidner, M. vd Lühe, et al., Intentional formation of a protein corona on nanoparticles: Serum concentration affects protein corona mass, surface charge, and nanoparticle-cell interaction., *Int J. Biochem Cell Biol.* (2015).
- [44] M. Nieh, J. Katsaras, X. Qi, Controlled release mechanisms of spontaneously forming unilamellar vesicles, *Biochim. Et. Biophys. Acta (BBA) - Biomembr.* 1778 (6) (2008) 1467–1471.
- [45] R. Hofheinz, S. Gnad-Vogt, U. Beyer, A. Hochhaus, Liposomal encapsulated anti-cancer drugs, *Anticancer Drugs* 16 (7) (2005).
- [46] M. Zborowski, J.J. Chalmers, Rare cell separation and analysis by magnetic sorting, *Anal. Chem.* 83 (21) (2011) 8050–8056.
- [47] P. Chen, Y. Huang, K. Hoshino, J.X.J. Zhang, Microscale magnetic field modulation for enhanced capture and distribution of rare circulating tumor cells, *Sci. Rep.* 5 (2015) 8745.
- [48] B. Sinha, S. Anandkumar, S. Oh, C. Kim, Micro-magnetometry for susceptibility measurement of superparamagnetic single bead, *Sens. Actuators A: Phys.* 182 (2012) 34–40.
- [49] D.J. Wever, A.G. Veldhuizen, M.M. Sanders, J.M. Schakenraad, J.R. van Horn, Cytotoxic, allergic and genotoxic activity of a nickel-titanium alloy, *Biomaterials* 18 (16) (1997) 1115–1120.
- [50] M. Alagiri, K. Ashok, C. Muthamizhchelvan, S. Ponnusamy, Observation of magnetic, structural and surface morphological studies of triangle-like nickel nanoplates, *Mater. Lett.* 65 (2) (2011) 310–313.
- [51] Y. Chen, D. Peng, D. Lin, X. Luo, Preparation and magnetic properties of nickel nanoparticles via the thermal decomposition of nickel organometallic precursor in alkylamines, *Nanotechnology* 18 (50) (2007) 505703.
- [52] S.N. Bhatia, U.J. Balis, M.L. Yarmush, M. Toner, Effect of cell-cell interactions in preservation of cellular phenotype: cocultivation of hepatocytes and nonparenchymal cells, *FASEB J.* 13 (14) (1999) 1883–1900.
- [53] M.W. Toepke, D.J. Beebe, PDMS absorption of small molecules and consequences in microfluidic applications, *Lab a Chip* 6 (12) (2006) 1484–1486.
- [54] V.J. Mohanraj, Y. Y. Chen, Nanoparticles: a review, *Trop. J. Pharm. Res.* 5 (1) (2006) 561–573.
- [55] R.H. Müller, K. Mäder, S. Gohla, Solid lipid nanoparticles (SLN) for controlled drug delivery – a review of the state of the art, *Eur. J. Pharm. Biopharm.* 50 (1) (2000) 161–177.
- [56] R.L. Rich, D.G. Myszka, Advances in surface plasmon resonance biosensor analysis, *Curr. Opin. Biotechnol.* 11 (1) (2000) 54–61.